RAA 2019 Vol. **19** No. **12**, 185(16pp) doi: 10.1088/1674–4527/19/12/185

http://www.raa-journal.org *http://iopscience.iop.org/raa*

Research in Astronomy and Astrophysics

Anisotropic turbulence of kinetic Alfvén waves and heating in solar corona

Hemam Dinesh Singh and Bheem Singh Jatav*

Department of Physics, Sikkim University, Gangtok, Sikkim, 737102, India; *hemamdine@gmail.com*

Received 2019 May 27; accepted 2019 July 9

Abstract Understanding solar coronal heating has been one of the unresolved problems in solar physics in spite of the many theories that have been developed to explain it. Past observational studies suggested that kinetic Alfvén waves (KAWs) may be responsible for solar coronal heating by accelerating the charged particles in solar plasma. In this paper, we investigated the transient dynamics of KAWs with modified background density due to ponderomotive force and Joule heating. A numerical simulation based on pseudo-spectral method was applied to study the evolution of KAW magnetic coherent structures and generation of magnetic turbulence. Using different initial conditions in simulations, the dependence of KAW dynamics on the nature of inhomogeneous solar plasma was thoroughly investigated. The saturated magnetic power spectra follow Kolmogorov scaling of $k^{-5/3}$ in the inertial range, then followed by steep anisotropic scaling in the dissipation range. The KAW has anisotropy of $k_\parallel \propto k_\perp^{0.53}$, $k_\parallel \propto k_\perp^{0.50}$, $k_\parallel \propto k_\perp^{0.83}$ and $k_\parallel \propto k_\perp^{0.30}$ depending on the kind of initial conditions of inhomogeneity. The power spectra of magnetic field fluctuations showing the spectral anisotropy in wavenumber space indicate that the nonlinear interactions may be redistributing the energy anisotropically among higher modes of the wavenumber. Therefore, anisotropic turbulence can be considered as one of the candidates responsible for the particle energization and heating of the solar plasmas.

Key words: plasmas — turbulence — waves — Sun: corona

1 INTRODUCTION

One of the fundamental unsolved issues of astrophysics is the solar coronal heating problem, where the outer atmosphere of the Sun has a high temperature corona of around 2×10^6 K as compared to the photosphere of around 6000 K. In the past few decades, many spacecraft observations from the *Solar and Heliospheric Observatory* (*SOHO*), *Transition Region and Coronal Explorer* (*TRACE*), *Hinode* and *Solar Dynamics Observatory* (*SDO*) have revealed that the solar atmosphere is in nature far from dynamical and thermal equilibrium. It has inhomogeneity in magnetic field and density. Therefore, the nonuniform heating processes of magnetoplasma fine structures play a very significant role in the coronal heating. These coherent structures or filaments are often identified as the manifestation of field aligned density (or temperature) striations and their heating mechanisms are closely related to solar magnetic fields.

The solar corona is generally divided into coronal holes (open regions) and coronal loops (closed regions). The cooler and less dense coronal holes are the sources of solar wind. The associated magnetic field lines are carried away from these regions to space by the solar winds through the escaping energetic particles. The first coronal heating mechanism involving the role of solar magnetic field lines was proposed by Alfvén (1942) using Alfvén waves (AWs). Since then many theories were put forward to explain the coronal heating and solar wind acceleration (Marsch 2006; Sirenko et al. 2002; Cranmer et al. 2007; Cranmer 2009). Among them, two prominent theories are: heating by waves (Narain & Ulmschneider 1996; Hood et al. 1997; Goossens 1994; Priest et al. 2000; Poedts et al. 1989; Ruderman 1999) and heating by flares or magnetic reconnection (Jain et al. 2005; Hood et al. 2009; Sturrock et al. 1999; Cassak & Shay 2012). However, there is still no universally accepted self-consistent model to explain the physical processes behind the coronal heating and solar wind acceleration. Recently, there are many observational and theoretical evidences showing that AWs are the main candidates for being able to transport sufficient energy in the solar atmosphere to reach the temperature of million Kelvins in the coronal regions (Parker 1979; De

* Supported by the RGNF, UGC, India.

Pontieu et al. 2007; Okamoto et al. 2007; Cirtain et al. 2007). However, since the perpendicular scale length of pure AWs is very large, their dissipation is insufficient to convert the wave energy to particle kinetic energy in the range of coronal temperature of million Kelvins (Wu & Chen 2013).

The AWs become dispersive and are called dispersive AWs (DAWs) when they have a short cross-field wavelength comparable to the main kinetic length scale of the plasma, λ_e or ρ_i or ρ_s (whatever is longer) where λ_e is the electron inertial length, ρ_i is the ion gyroradius and ρ_s is the ion acoustic gyroradius. Subsequently the inertial AW (IAW) can be defined as a DAW when $\lambda_e > \rho_i$ or ρ_s and the kinetic AW (KAW) when $\rho_s >$ or $\rho_i > \lambda_e$. Due to the dispersive nature of DAWs, they are rapidly damped and can play an important role in inhomogeneous coronal heating (de Azevedo et al. 1994; Voitenko 1995; Voitenko 1996; Elfimov et al. 1996; Asgari-Targhi & van Ballegooijen 2012; Morton et al. 2015; Testa et al. 2014).

In the magnetohydrodynamics (MHD) regime, AWs cannot develop field aligned electric fields which can accelerate and heat the charged particles (Stéfant 1970). If plasma is treated as a collection of charged particles (kinetic regime) instead of as fluid in MHD, then the field aligned electric fields are developed, thus producing anisotropic and mass-dependent energization of heavy ions (Voitenko & Goossens 2004; Wu & Yang 2006). When DAWs propagate in the transversely homogeneous plasma, the parallel electric fields generated in the region of plasma inhomogeneity can effectively accelerate the charge particles (Tsiklauri & Haruki 2008). Hasegawa & Chen (1975) performed an experiment to convert the AW mode to KAW by applying a resonant oscillating magnetic field of frequency near 1 MHz. In space plasmas also, this kind of resonant mode conversion to DAWs is found when surface waves are excited either by an MHD plasma instability or an externally applied impulse (Tsiklauri 2011). The physical mechanism for producing parallel electric fields in DAWs can be understood considering a two fluid model of plasma. This can be supported by either a parallel electron inertia term (as in the case of IAWs) or parallel electron pressure gradient term (as in case the of KAWs) appearing in the electron equation of motion. For IAWs the Alfvén speed is much greater than ion and electron thermal speeds, thereby giving the plasma β much less than electron to ion mass ratio m_e/m_i where $\beta = 8\pi n_0 T/B_0^2$ (thermal to magnetic pressure ratio), n_0 is the unperturbed plasma number density, $T(= T_e \approx T_i)$ is the plasma temperature and B_0 is the external ambient direct current (DC) magnetic field. For KAWs, the thermal speed is much grater than the Alfvén speed, so the plasma $\beta << m_e/m_i$.

The mechanism of phase mixing, in which an AW propagates across an inhomogenous density that is transverse to the background ambient magnetic field, can transfer the wave energy from large scales to small scales in the transverse direction of the magnetic field. The phase mixing effect leads to the formation of transverse magnetic wavefronts (magnetic coherent structures or filaments). This provides a fast dissipation mechanism for coronal heating and solar wind acceleration. Tsiklauri et al. (2005) studied the solar coronal plasma and found that phase mixing of the KAWs can effectively accelerate the electrons. In the magnetospheric plasma regions, this kind of particle accelerations was also found (Génot et al. 1999; Génot et al. 2004; Mottez et al. 2006). Mottez & Génot (2011) studied numerically the interaction of an isolated IAW packet with a plasma density cavity and formation of small scale coherent electric structures.

Recently, the process of particle acceleration by polarized DAWs in a transversely inhomogeneous plasma was investigated by Tsiklauri (2011) and Tsiklauri (2012) using 2.5D and three-dimensional (3D) particle-in-cell simulation. From many studies we can conclude that DAWs of low frequency ($\omega < \omega_{ci}$ where $\omega_{ci} = eB/m_i$ is ion cyclotron frequency), propagating in a transversely inhomogeneous plasma when the transverse density (or/and temperature) inhomogeneity scale is comparable to the microscopic scales of particle motions (electron inertial or ion gyroradius length), generate sufficient parallel and perpendicular components of electric fields to efficiently accelerate the electrons and ions in parallel and perpendicular directions of the ambient magnetic fields respectively.

The IAWs are applicable to plasmas to very low values of β, $\beta < m_e/m_i$. In the auroral zones of the terrestrial magnetosphere at heights below four Earth radii, this condition is satisfied, but in the solar corona the commonly accepted typical values of β are between m_e/m_i and 1, both in active regions and coronal holes. However, the condition $\beta < m_e/m_i$ is satisfied at the base of the coronal hole or hole loop where the heavy particle density $n_0 \sim (10^8 - 10^{10})\,\mathrm{cm}^{-3}$ and ambient magnetic field $B_0 \sim (5 - 150)\,\mathrm{G}$ (Champeaux et al. 1997). On comparing the possible parameter values of the solar wind and coronal loops, KAW is applicable in both the regions, i.e. $m_e/m_i << \beta << 1$, where the solar wind $\beta = 0.121$ at 1 AU (Cravens 2004) and the coronal loops $\beta = 0.01$ (Shukla et al. 1999a,b). The magnetic field of the solar wind ($B_0 \approx 1 \times 10^{-4}\,\mathrm{G}$) is considerably less than that of the coronal loop $B_0 \approx 100\,\mathrm{G}$. Similarly, the density of the coronal plasma ($n_0 \approx 5 \times 10^9\,\mathrm{cm}^{-3}$) is much higher than that of solar wind ($n_0 \approx 5\,\mathrm{cm}^{-3}$). Temperatures of both the regions are very much similar and they are of the orders of million Kelvins. Similarly, the ion to electron temperature ratios of both the regions are approximately same.

Wu & Chen (2013) also studied the instability of KAWs driven by transverse density gradient and showed that the instability has the maximal growth rate at the perpendicular wavelength close to the spatial characteristic scale of the density gradient. The transverse density fluctuations are always with KAWs because of their strong anisotropy (with the perpendicular wavelengths being much shorter than parallel ones) and coupling with strong electrostatic modes. Sahraoui et al. (2010) investigated the spectrum of turbulence and demonstrated that highly oblique KAWs are responsible for strong anisotropy.

The nonlinear evolution of turbulent saturated spectra of KAWs can only be studied by cascade process or filamentation process. Voitenko (1996); Voitenko (1998) first investigated excitation of KAWs by flare-producing energetic proton beams and concluded that KAW instability is an efficient energy conversion mechanism in coronal loops and solar flares. Furthermore, many theoretical studies also indicated that the dissipation of KAWs can efficiently provide inhomogeneous heating in bright coronal loops (Wu & Fang 1999), bright coronal plumes (Wu & Fang 2003), sunspot chromosphere (Wu & Fang 2007), and anisotropic and mass dependent heating in the solar corona (Wu & Yang 2006; Wu & Yang 2007). All these demonstrate that KAWs possibly play an important role in heating the solar corona and accelerating the solar wind. Many authors (Wu et al. 1997; Wang et al. 1998; Chen et al. 2000) have examined the solitary KAWs having density solitons (dip, hump and dipole) to account for observations from the *Freja* satellite and found that it can lead to auroral particle acceleration and coronal heating. Bellan & Stasiewicz (1998) derived the analytical expression for ponderomotive force associated with KAWs. Further, Shukla & Stenflo (2000b) showed that the ponderomotive force of KAWs can generate magnetic field-aligned quasistationary density humps and dips.

Many of the theories of AW turbulence (Goldreich & Sridhar 1995; Goldreich & Sridhar 1997) predicted that the turbulent process of AWs causes the wave energy to cascade, predominantly in the transverse direction to the field lines, i.e. $k_\perp >> k_\|$, where $k_\perp$ ($k_\|$) is the wavenumber perpendicular (parallel) to the ambient magnetic field. As $k_\perp$ increases (i.e., the perpendicular wavelength decreases), the AWs become more and more anisotropic (Howes et al. 2006; Schekochihin et al. 2009). Various numerical studies (Maron & Goldreich 2001; Cho et al. 2002) and spacecraft data (Leamon et al. 1998; Luo & Wu 2010; Luo et al. 2011) confirmed the anisotropically cascading model of AW turbulence. The cross field density fluctuations are always with KAWs because of their strong anisotropy. Therefore, the effect of finite $k_\perp \rho_s$, i.e. $\partial/\partial x >> \partial/\partial z$, (ambient magnetic field in the z-direction) becomes significant in the dynamics of nonlinear KAWs.

The objective of the present work is to investigate the transient KAW dynamics propagating in an inhomogeous plasma arising from the field aligned density fluctuations because of ponderomotive force and Joule heating. The dynamical field equation satisfies a modified nonlinear Schrödinger equation (NLSE). The dynamical field equation couples with the field aligned density perturbations, thereby the nonlinearity in the field equation leads to localization of KAW wave packet as envelope solitons. As the wave propagates, the transverse collapse of the coherent structures happens and the energy is dissipated from large scale to small scale via small wavenumber to high wavenumber space. The numerical simulation employing the pseudo-spectral method was carried out with the possible parameters of coronal loop plasma to study the formation of the coherent magnetic field structures, cascade of energy at different wavenumbers and the effect of initial plasma inhomogeneities. Transverse collapse of the field aligned magnetic coherent structures is one of the efficient mechanisms to transfer energy from large scale to small scale, as asymptotically predicted by the NLSE for the wave envelope (Champeaux et al. 1998; Laveder et al. 2001). Therefore, the magnetic coherent structures (filaments) generated by KAWs play an important role in explaining the dissipation range of the turbulent spectra of solar coronal regions. Many authors have already examined the dynamics of KAW in the form of modified NLSE to investigate the coronal heating and solar wind acceleration. Sharma et al. (2006); Singh & Sharma (2007); Singh & Jatav (2019) studied the steady state dynamical equations satisfied by KAWs leading to the intense magnetic filaments. However, these investigations were limited to stationery states only and much about the anisotropic nature of the magnetic fluctuations was not discussed. In reality, waves are time dependent. Therefore, this paper focuses on the transient propagation of two-dimensional (2D)-KAWs in coronal plasma and the effect of changing the initial perturbations on the formation of magnetic filaments and the anisotropic wavenumber spectral indices. The interactions of 3D-KAWs and 3D-ion acoustic waves and their role in the localization and heating of KAWs in solar plasma have been numerically addressed by Sharma et al. (2014); Sharma et al. (2016). They proposed the evolution of KAW vortices as a result of twisting the magnetic filaments as the main source of solar plasma heating. As the coronal loops are progressively twisted with the evolution in time, the current flowing in the plasma channel will increase. Once the current reaches the critical value, the flares will occur. There is no single clear physical mechanism which produces the small scale fluctuations leading to plasma heating. It may be due to KAWs or whistler waves, or the interactions between them (Gary & Smith 2009; Salem et al. 2012; Boldyrev et al. 2013; Chen et al. 2013a,b) or interactions of KAWs with ion acoustic or magnetosonic waves (Sharma et al. 2017). Therefore, the KAW propagation in the modified background density due to ponderomotive force and Joule heating, as we discussed here, leading to the transverse collapse of magnetic coherent structures may be one of the possible physical processes to explain the heating in coronal loops.

The sections of this paper are divided as follows. The model equation satisfied by KAWs in the solar corona is described in Section 2. The numerical results depicted as magnetic field intensity profile and magnetic spectra are presented in Section 3, comparing it with previous studies and spacecraft observations. In Section 4, we discuss the overall conclusions.

2 MODEL KAW DYNAMICS

Let us consider a low frequency KAW propagating in the x-z plane ($\boldsymbol{k_0} = k_{0x}\hat{x} + k_{0z}\hat{z}$). We assume the ambient DC magnetic field B_0 along the z-axis ($\boldsymbol{B_0} = B_0\hat{z}$) and the plasma β range as ($m_e/m_i << \beta << 1$). The momentum balance equation and field equations are written in the two fluid model. To apply the procedure of linearization in the equations, the parameters of the medium (e.g. density, velocity and the electromagnetic fields) are separated into an equilibrium (undisturbed) part indicated by the subscript 0 and a superimposed disturbance (perturbation) part indicated by the subscript 1.

$$n = n_0 + n_1, \boldsymbol{v} = \boldsymbol{v}_0 + \boldsymbol{v}_1, \boldsymbol{E} = \boldsymbol{E}_0 + \boldsymbol{E}_1, \boldsymbol{B} = \boldsymbol{B}_0 + \boldsymbol{B}_1 \tag{1}$$

In the equilibrium plasma, the undisturbed density, velocity and fields are constant and uniform, i.e.

$$\boldsymbol{\nabla} n_0 = \boldsymbol{v}_0 = \boldsymbol{E}_0 = 0 \tag{2}$$

and

$$\frac{\partial n_0}{\partial t} = \frac{\partial \boldsymbol{v}_0}{\partial t} = \frac{\boldsymbol{E}_0}{\partial t} = 0. \tag{3}$$

By applying the procedure of linearization, we neglect the terms containing higher powers of the perturbating amplitude factors and write the equations as:

Equation of motion:

$$\frac{\partial \boldsymbol{v_{j1}}}{\partial t} \approx \frac{q_j}{m_j}\boldsymbol{E}_1 + \frac{q_j}{cm_j}(\boldsymbol{v_{j1}} \times \boldsymbol{B_0}) - \frac{\gamma_j k_B T_j}{n_{j0} m_j}\boldsymbol{\nabla} n_{j1}. \tag{4}$$

Continuity equation:

$$\frac{\partial n_{j1}}{\partial t} + n_{j0}\boldsymbol{\nabla}\cdot\boldsymbol{v}_{j1} \approx 0. \tag{5}$$

Faraday's law:

$$\boldsymbol{\nabla} \times \boldsymbol{E}_1 = -\frac{1}{c}\frac{\partial \boldsymbol{B_1}}{\partial t}. \tag{6}$$

where the subscript j denotes e (electrons) and i (ions), $\boldsymbol{v}$ is the velocity, q is the charge, m is the mass, c is the speed of light in a vacuum, γ (c_p/c_v) is the ratio of the specific heats and k_B is the Boltzmann constant. Here n denotes the plasma number density with quasineutrality condition, i.e. $n_{e0} \simeq n_{i0} \simeq n_0$ and $n_{e1} \simeq n_{i1} \simeq n_1$. We take the isothermal condition $\gamma_e = \gamma_i = 1$.

From the force Equation (4), the perpendicular components of the electron and ion velocities under the KAW low frequency approximation ($\omega << \omega_{ci}$ and $\omega << \omega_{ce}$ where $\omega_{ci} = eB_0/m_ic$ and $\omega_{ce} = eB_0/m_ec$ are the ion and electron cyclotron frequencies respectively) are as follows:

$$(\boldsymbol{v}_{e1})_\perp \approx \frac{c}{B_0}\boldsymbol{E}_{1\perp} \times \hat{z} - \frac{k_BT_e}{m_e\omega_{ce}n_0}\hat{z} \times \boldsymbol{\nabla}_\perp n_1 \tag{7}$$

and

$$\begin{aligned}(\boldsymbol{v}_{i1})_\perp \approx \frac{e}{\omega_{ci}m_i}\Big[\boldsymbol{E}_{1\perp} - \frac{k_BT_i}{en_0}\boldsymbol{\nabla}_\perp n_1\Big] \times \hat{z} \\ - \frac{i\omega}{\omega_{ci}^2}\frac{e}{m_i}\Big[\boldsymbol{E}_{1\perp} - \frac{k_BT_i}{en_0}\boldsymbol{\nabla}_\perp n_1\Big].\end{aligned} \tag{8}$$

The parallel electron velocity can be found from

$$\frac{\partial (v_{e1})_z}{\partial t} = \frac{-eE_{1z}}{m_e} - \frac{k_BT_e}{m_en_0}\frac{\partial n_1}{\partial z}. \tag{9}$$

The current density is given by

$$\boldsymbol{J} \approx en_0(\boldsymbol{v}_{i1} - \boldsymbol{v}_{e1}). \tag{10}$$

After this, we will not again use the subscript "1" in denoting the varying (perturbing) parts of $\boldsymbol{v}$, $\boldsymbol{E}$ and $\boldsymbol{B}$ except in denoting the varying part of n.

The y-component of Faraday's law is

$$\frac{1}{c}\frac{\partial B_y}{\partial t} = \frac{\partial E_z}{\partial x} - \frac{\partial E_x}{\partial z}. \tag{11}$$

Taking the conservation of current density, $\boldsymbol{\nabla}\cdot\boldsymbol{J} = 0$, and also by using $J_z \approx -en_0v_{ez}$ and $\boldsymbol{J}_\perp \approx en_0(\boldsymbol{v_{i\perp}} - \boldsymbol{v_{e\perp}})$, we get

$$\frac{\partial^2 E_x}{\partial x \partial t} = \frac{B_0\omega_{ci}}{c}\Big(\frac{\partial v_{ez}}{\partial z}\Big). \tag{12}$$

Taking the z-component of Ampere's law and eliminating the parallel component of current density and substituting it in Equation (12), we obtain,

$$\frac{\partial E_x}{\partial t} = -\frac{v_A^2}{c}\Big(1 - \frac{n_1}{n_0}\Big)\frac{\partial B_y}{\partial z}, \tag{13}$$

where $v_A(= \sqrt{B_0^2/4\pi n_0 m_i})$ is the AW speed.

Now we can find the time derivative of parallel electric field from the parallel component of Ampere's law and substituting therein the parallel electron fluid velocity given by Equation (9) and the continuity Equation (5), we arrive at

$$\frac{\partial E_z}{\partial t} = -\frac{v_{te}^2 \lambda_e^2}{c} \frac{\partial}{\partial x} \frac{\partial^2 B_y}{\partial z^2}, \tag{14}$$

where $\lambda_e (= c/\omega_{pe})$ represents the electron inertial length or collisionless skin depth, $\omega_{pe} (= \sqrt{4\pi n_0 e^2/m_e})$ signifies the frequency for electron plasma oscillation and $v_{te}\left(= \sqrt{\frac{k_B T_e}{m_e}}\right)$ corresponds to the electron thermal speed.

Taking the time derivative of Equation (11) and substituting therein the z-derivative of Equation (13) and the x-derivative of Equation (14), we get the following dynamical equation (Hasegawa & Chen 1975; Bellan & Stasiewicz 1998; Shukla et al. 1999a,b; Shukla & Stenflo 2000a,b; Sharma & Kumar 2011)

$$\frac{\partial^2 B_y}{\partial t^2} = -v_A^2 \rho_s^2 \frac{\partial^4 B_y}{\partial x^2 \partial z^2} + v_A^2 \Big(1 - \frac{n_1}{n_0}\Big) \frac{\partial^2 B_y}{\partial z^2}, \tag{15}$$

where ρ_s $(= \lambda_e v_{te}/v_A = c_s/\omega_{ci})$ represents the ion acoustic gyroradius at electron temperature and c_s $(= \sqrt{k_B T_e/m_i})$ signifies the ion sound speed.

By applying a Fourier transform to Equation (15), the dispersion relation of KAWs for $m_e/m_i << \beta << 1$ can be obtained (Shukla & Stenflo 2005) as

$$\frac{\omega^2}{k_{0z}^2 v_A^2} = 1 + k_{0x}^2 \rho_s^2. \tag{16}$$

One of the possible solutions of Equation (15) is a plane wave (linear polarization) modulated by a slowly varying envelope $B_y'(x, z)$ which is expressed as

$$B_y = B_y'(x, z, t) e^{i(k_{0x}x + k_{0z}z - \omega t)} \tag{17}$$

where $B_y'(x, z, t)$ is the amplitude of the transverse KAW magnetic field. It is varying slowly in spatial coordinates in comparison to the exponential part $e^{i(k_{0x}x+k_{0z}z-\omega t)}$. We substitute it in Equation (15) to produce

$$\begin{aligned} &i\frac{2\omega}{v_A^2 k_{0z}^2}\frac{\partial B_y'}{\partial t} + i\frac{2}{k_{0z}}\frac{\partial B_y'}{\partial z} + \rho_s^2 \frac{k_{0x}^2}{k_{0z}^2}\frac{\partial^2 B_y'}{\partial z^2} \\ &+ \rho_s^2 \frac{\partial^2 B_y'}{\partial x^2} + 2ik_{0x}\rho_s^2 \frac{\partial B_y'}{\partial x} + \frac{n_1}{n_0} B_y' = 0. \end{aligned} \tag{18}$$

In a nonuniform, inhomogeneous plasma medium, if the amplitudes of the waves are spatially varying, the nonlinear magnetic gradient produces a force known as the ponderomotive force. The plasma density can be modified by the combined effects of ponderomotive force and Joule heating generated from plasma currents (Shukla & Stenflo 1999). When large amplitude KAWs propagate, the variations in plasma density in the form of field aligned density humps and dips have been reported in the laboratory and space plasmas (Gekelman et al. 1999). This variation in particle density under adiabatic approximation (slowly varying in time with respect to density fluctuations) was calculated as (Shukla & Stenflo 2000a)

$$n_1 \approx n_0 \Big(e^{\xi |B_y'|^2} - 1\Big), \tag{19}$$

where $\xi = \{[1 - \Delta(1+\delta) v_A^2 k_{0z}]/16\pi n_0 T_e \omega^2\}$, $\Delta = \omega^2/\omega_{ci}^2$ and $\delta = m_e k_{0x}^2/m_i k_{0z}^2$. In case of $\omega\ (1+\delta)^{1/2} < \omega_{ci}$ the density change is a hump. For plasma $\beta >> m_e/m_i$, we get v_{ti} and $v_{te} > v_A$. Therefore, the electrons or ions can move fast enough to respond to any adiabatic changes in density.

We can reduce Equation (18) in dimensionless form with the substitution of Equation (19) and it becomes

$$\begin{aligned} &i\frac{\partial B_y'}{\partial t} + i\frac{\partial B_y'}{\partial z} + 2iK\frac{\partial B_y'}{\partial x} + K^2 \frac{\partial^2 B_y'}{\partial z^2} \\ &+ \frac{\partial^2 B_y'}{\partial x^2} + \frac{1}{2g}\Big(e^{2g|B_y'|^2} - 1\Big) B_y' = 0, \end{aligned} \tag{20}$$

where we represent the normalized transverse wavenumber as $K = k_{0x}\rho_s$ and the other normalizing parameters are $t_n = 2\omega/v_A^2 k_{0z}^2$, $z_n = 2/k_{0z}$, $x_n = \rho_s$ and $B_n = [\{1 - \Delta(1+\delta)\} V_A^2 k_{0z}^2/16\pi n_0 T_e \omega^2]^{-1/2}$. The dimensionless parameter g was introduced for the sake of generality. By varying the parameter g, we can control the amplitude of the pump KAW. In other words, we can say that this parameter controls the coupling between the density perturbation and magnetic field. In the case of $g = 0$, the density profile becomes quadratic in magnetic field and Equation (20) assumes the form of a modified cubic NLSE type. If we increase g, the system behaves as chaotic. These were studied earlier by one of the authors of this paper (Sharma et al. 2006; Singh & Sharma 2007), but they were limited to only steady states. The waves are actually transient in nature. Therefore, the time evolution of KAWs applicable in solar plasma is studied numerically herewith.

To correlate the parameter g with KAW pump amplitude, we consider a simpler homogeneous solution of Equation (20) with $K = 0$ as $B_{y0}e^{-iz}$ (Zhou et al. 1992; Zhou & He 1994) and we get

$$|B_{y0}| = \sqrt{\frac{\ln|1 - 2g|}{2g}} \tag{21}$$

where $0 \leq g < 1/2$ and B_{y0} is the amplitude of the homogeneous pump KAW.

3 NUMERICAL SIMULATION AND RESULTS

The numerical simulation of Equation (20) was performed by using a fully dealiased 2D pseudo-spectral method for spatial integration with periodic spatial domain of $L_x = 2\pi/\alpha_x$ and $L_z = 2\pi/\alpha_z$ (where α_x and α_z are the perturbation wavenumbers in x and z directions respectively) with $2^7 \times 2^7$ grid points and a modified version of the Gazdag predictor corrector method for evolution in time with a step size of $dt = 5 \times 10^{-5}$. First we wrote the algorithm for the well-known 2D-cubic NLS equation. The linear terms were solved in Fourier space by applying the Fast Fourier Transform (FFT). For the nonlinear term, the local product in real space was taken first and then the FFT was applied to transform it into Fourier space. Since the linear evolution is exactly integrable, a plane wave is a possible solution. Having the plane wave solution is an important feature of the code and it helps in reproducing other features like instabilities. Next, we modified the algorithm to numerically solve our desired Equation (20).

To understand the role of the initial conditions of the inhomogenous magnetic field in time evolution of KAWs when the field aligned density perturbations are taken into account, we implemented four kinds of initial conditions in the simulations. First, we use a uniform plane KAW of fixed amplitude superimposed by a sinusoidal periodic perturbation, which is denoted hereafter as IC-1.

$$B'_y(x,z,t=0) = B_{y0}\left[1+\varepsilon\ \cos(\alpha_x x)\right] \times \left[1+\varepsilon\cos(\alpha_z z)\right] \quad (\mathrm{IC}-1)$$

where ε is the magnitude of the perturbation. The wavenumbers of the perturbations α_x and α_z are normalized by x_n^{-1} and z_n^{-1} respectively. The waves are really much more complicated than the sinusoidal waves, but all the waves can be represented as the sum of sinusoidal wave components.

When a Gaussian perturbation is superimposed on a uniform plane KAW, we denote it as IC-2.

$$B'_y(x,z,t=0) = B_{y0}\left[1+\varepsilon\ \exp\left(-x^2/r_{01}^2\right)\right] \times \left[1+\varepsilon\ \exp\left(-z^2/r_{02}^2\right)\right] \quad (\mathrm{IC}-2)$$

where r_{01} (normalized by x_n) and r_{02} (normalized by z_n) are the transverse and longitudinal scale sizes of the perturbations respectively.

For the third initial condition (IC-3), we applied a pump KAW of Gaussian wavefront and a sinusoidal perturbation superimposed on it.

$$B'_y(x,z,t=0) = B_{y0}\left[\exp(-x^2/r_0^2)+\varepsilon\cos(\alpha_x x)\right] \times \left[\exp(-z^2/r_0^2)+\varepsilon\cos(\alpha_z z)\right] \quad (\mathrm{IC}-3)$$

where r_0 (normalized by x_n) represents the transverse scale size of the main KAW initial beam width.

The last initial condition (IC-4) is a random perturbation superimposed on the Gaussian wavefront.

$$B'_y(x,z,t=0) = B_{y0}\left[\exp(-x^2/r_0^2)+\varepsilon\ \exp(2\pi i\theta(x))\right] \times \left[\exp(-z^2/r_0^2)+\varepsilon\ \exp(2\pi i\theta(z))\right] \quad (\mathrm{IC}-4)$$

where $\theta(x)$ and $\theta(z)$ are the random variables uniformly distributed on [0,1].

The parameter values we employed were $\varepsilon = 0.1$ and $\alpha_x = \alpha_z = 0.5$ so that all fields may be represented as discrete Fourier series with integral wave vector components. Furthermore, $r_0 = 1.0$ and $r_{01} = r_{02} = 5$, yielding $L_x = L_z \simeq 12.5 \simeq 2.5r_{01} \simeq 2.5r_{02}$. We have chosen a fixed value of $g = 0.01$, giving the amplitude of the pump wave $B_{y0} \simeq 1.005$. This produces the magnetic fluctuation $|\delta B_y/B_{y0}| \simeq 0.1$.

The coronal plasma parameters applicable to the intermediate plasma β are (Shukla et al. 1999a,b): $B_0 \approx 100\,G$, $n_0 \approx 5\times10^9\,\mathrm{cm}^{-3}$, $T_e \approx 6\times10^6\,\mathrm{K}$ and $T_i \approx 2\times10^6\,K$. Accordingly, we found $\beta = 0.01$, $v_{te} \approx 2\times10^9\,\mathrm{cm\,s}^{-1}$, $V_A \approx 3\times10^8\,\mathrm{cm\,s}^{-1}$, $\rho_s = 22\,\mathrm{cm}$ and $\rho_i = (\sqrt{T_i/T_e})\rho_s = 68\,\mathrm{cm}$. By taking $\omega/\omega_{ci} \approx 0.02$ and for $k_{0x}\rho_s \approx 0.01$ we get $k_{0x} \approx 1.9\times10^{-5}\,\mathrm{cm}^{-1}$, $k_{0z} \approx 1.5\times10^{-5}\,\mathrm{cm}^{-1}$. The normalized values are $x_n = 22\,\mathrm{cm}$, $z_n = 1.3\times10^5\,\mathrm{cm}$, $t_n = 1.4\times10^{-3}\,\mathrm{s}$ and $B_n = 0.91\,\mathrm{G}$. The parameters which have not been defined earlier are: ion gyroradius $\rho_i\ (= v_{ti}/\omega_{ci})$ and electron gyroradius $\rho_e\ (= v_{te}/\omega_{ce})$.

Here, we present the numerical simulation results for localization of KAWs and its dependence on initial conditions of simulations. The 2D snapshots of the time evolution of transverse KAW field intensity for various kinds of initial conditions are shown in Figures 1(a)–1(c), 2(a)–2(c), 3(a)–3(c) and 4(a)–4(c) at three instants of time. Due to ponderomotive force, which is exerted by the pump wave, the background density changes. The background density variations change the phase velocity of KAWs, which results in localization of the KAWs. The perturbation associated with the pump wave removes the energy and the coherent magnetic structures collapse with the evolution of time. Further, because of the nonlinear interactions of density and magnetic fields, collapsed structures try to regroup as time evolves. This process repeats until the evolution is not fully chaotic. For IC-1, at $t = 2$, the peak intensity of around 106 is formed at $(x = 0.78, z = 3.04)$. Because of the perturbation superimposed on the pump KAWs, ponderomotive force which is changing with time modifies the background density. The nonlinear coupling between the inhomogeneous density and the KAW magnetic field leads to the localization of KAWs and the perturbations of the magnetic field trigger the breakup of filamentary structures once they reach sufficient energy. This breakup is evident from Figure 1(b) of magnetic field profile at $t = 3$ forming the low and high intensity fil-

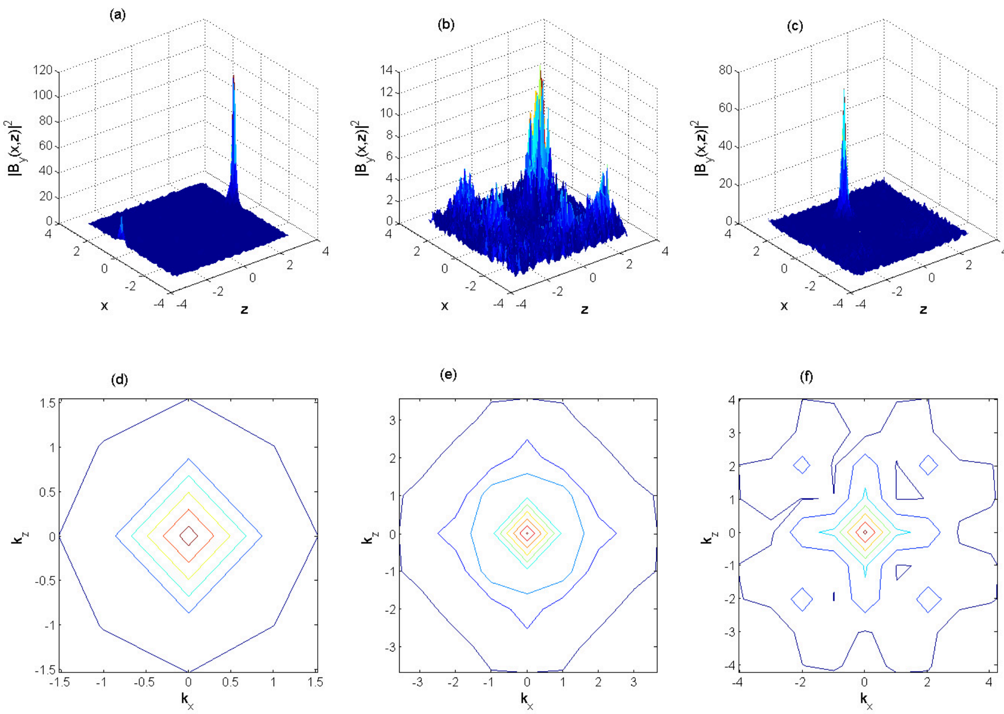

Fig. 1 Snapshots of normalized magnetic field intensity profiles (*upper panels*) and spectral contour plots of magnetic field intensity (*lower panels*) at $t = 2, 3$ and 4 for IC-1.

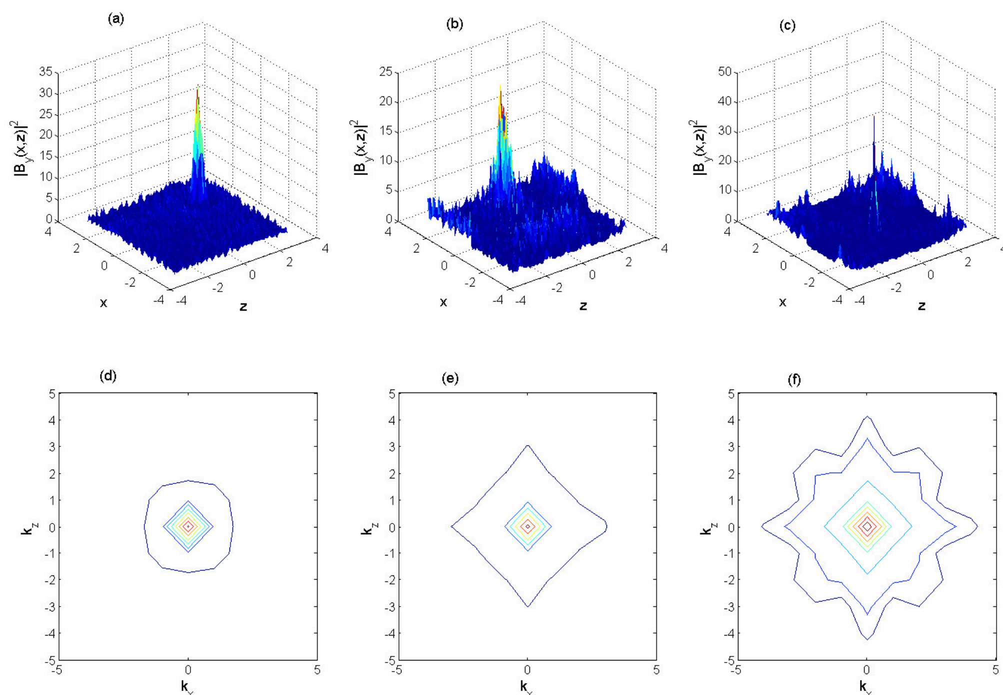

Fig. 2 Snapshots of normalized magnetic field intensity profiles (*upper panels*) and spectral contour plots of magnetic field intensity (*lower panels*) at $t = 3, 4$ and 6 for IC-2.

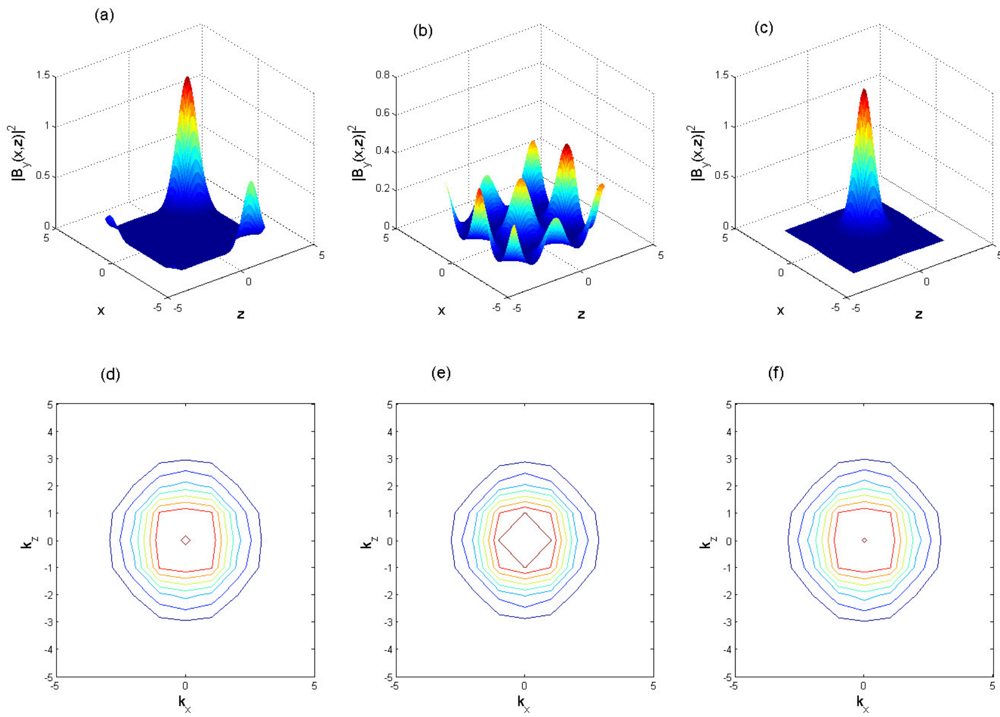

Fig. 3 Snapshots of normalized magnetic field intensity profiles (*upper panels*) and spectral contour plots of magnetic field intensity (*lower panels*) at $t = 6.5, 8$ and 9.5 for IC-3.

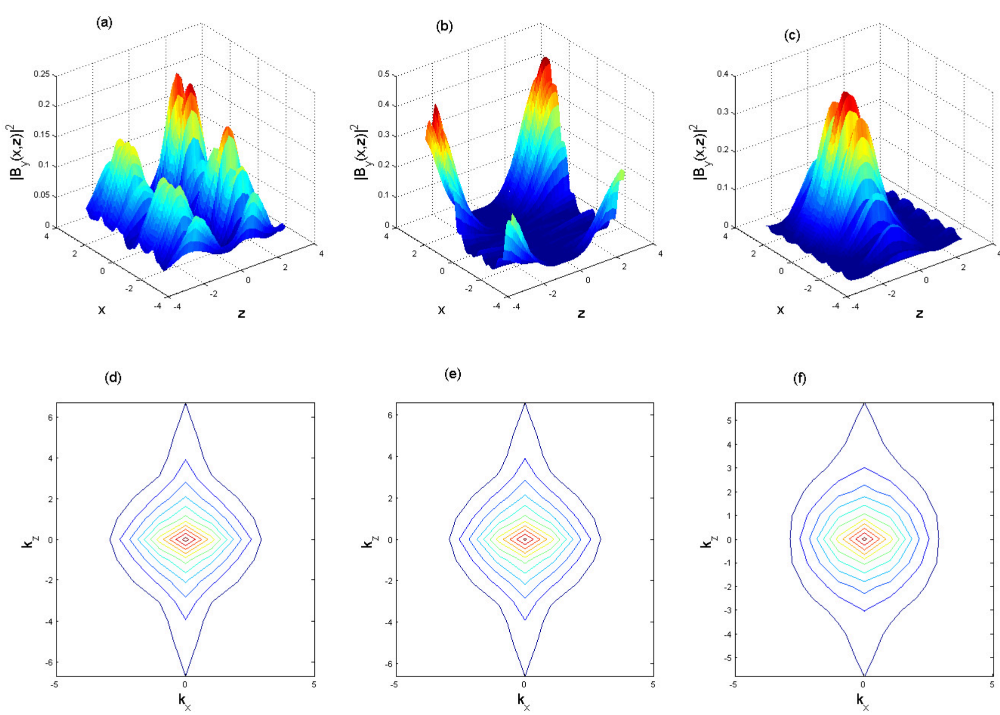

Fig. 4 Snapshots of normalized magnetic field intensity profiles (*upper panels*) and spectral contour plots of magnetic field intensity (*lower panels*) at $t = 5, 6$ and 10 for IC-4.

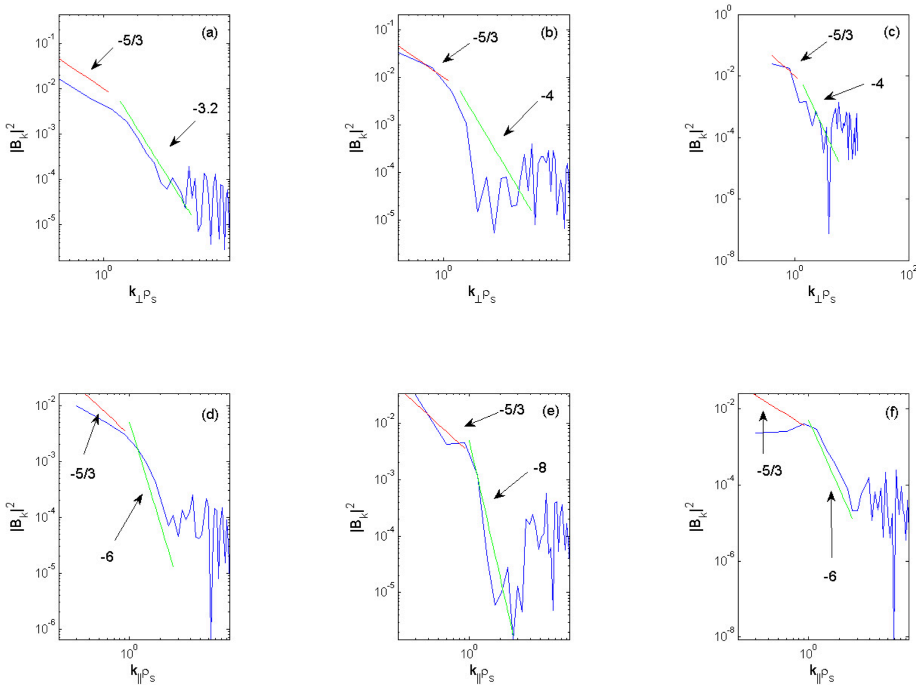

Fig. 5 Spectra of magnetic field fluctuations for IC-1 in $k_\perp$ space (*upper panels*) and $k_\parallel$ space (*lower panels*) at $t = 2$, 3 and 4.

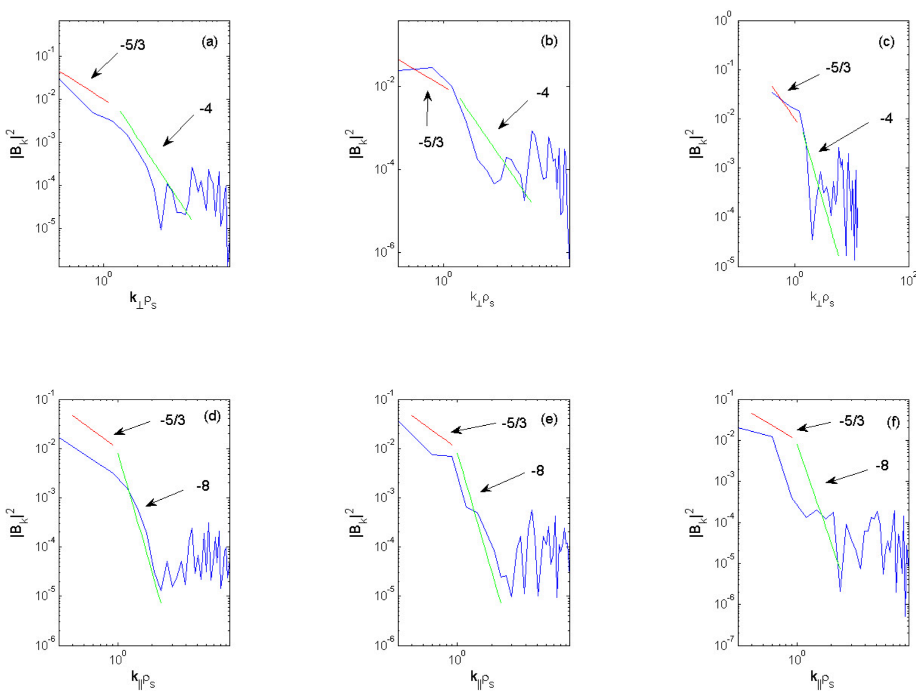

Fig. 6 Spectra of magnetic field fluctuations for IC-2 in $k_\perp$ space (*upper panels*) and $k_\parallel$ space (*lower panels*) at $t = 3$, 4 and 6.

aments at random locations in the (x, z) plane. Here the highest filament intensity of around 12.3 is formed at the location $(0.98, 1.57)$. At time $t = 4$, some of the scattered filaments regroup to form high intensity filaments and some filaments collapse to very low intensity filaments. The distributions of magnetic field intensity pattern in Fourier modes (k_x, k_z) are displayed in Figure 1(d)–1(f). Initially, the magnetic energy was confined to low

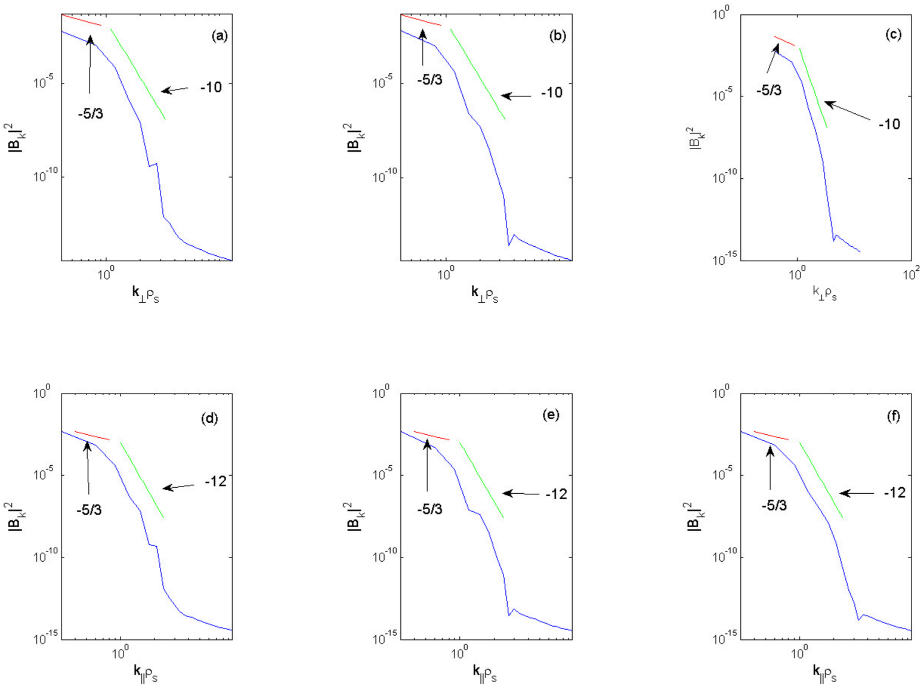

Fig. 7 Spectra of magnetic field fluctuations for IC-3 in $k_\perp$ space (*upper panels*) and $k_\parallel$ space (*lower panels*) at $t = 6.5$, 8 and 9.5.

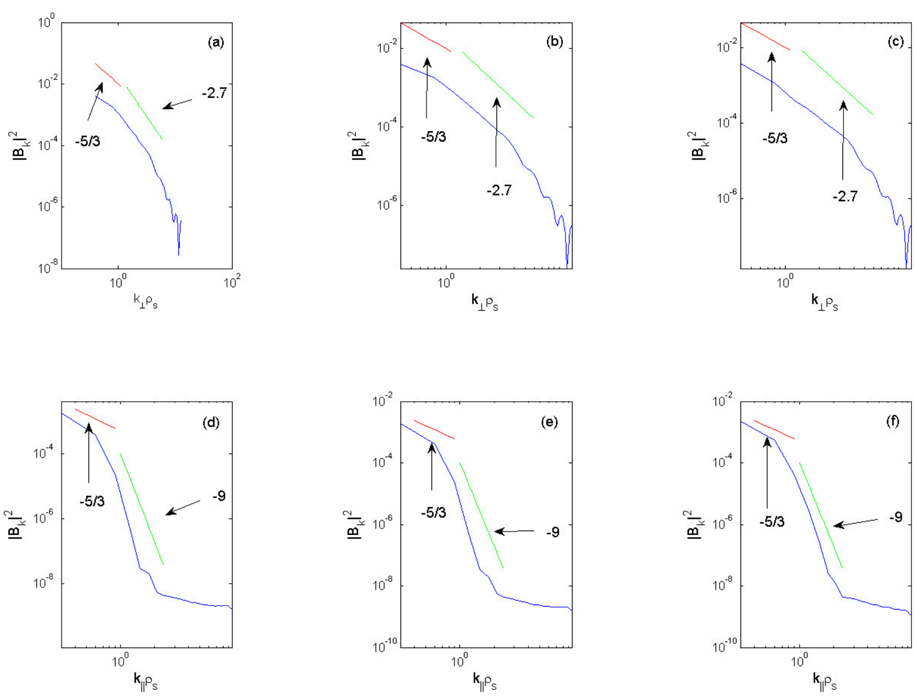

Fig. 8 Spectra of magnetic field fluctuations for IC-4 in $k_\perp$ space (*upper panels*) and $k_\parallel$ space (*lower panels*) at $t = 5$, 6 and 10.

wavenumber modes. As time evolves with the collapse of localized structures, the magnetic energy is distributed to higher wavenumber modes.

In Figure 2(a)–2(c), the simulation results for IC-2 are represented as snapshots of the 2D spatial evolution of KAWs at different times. Here nonuniformity in the KAWs is produced by the superposition of a Gaussian perturba-

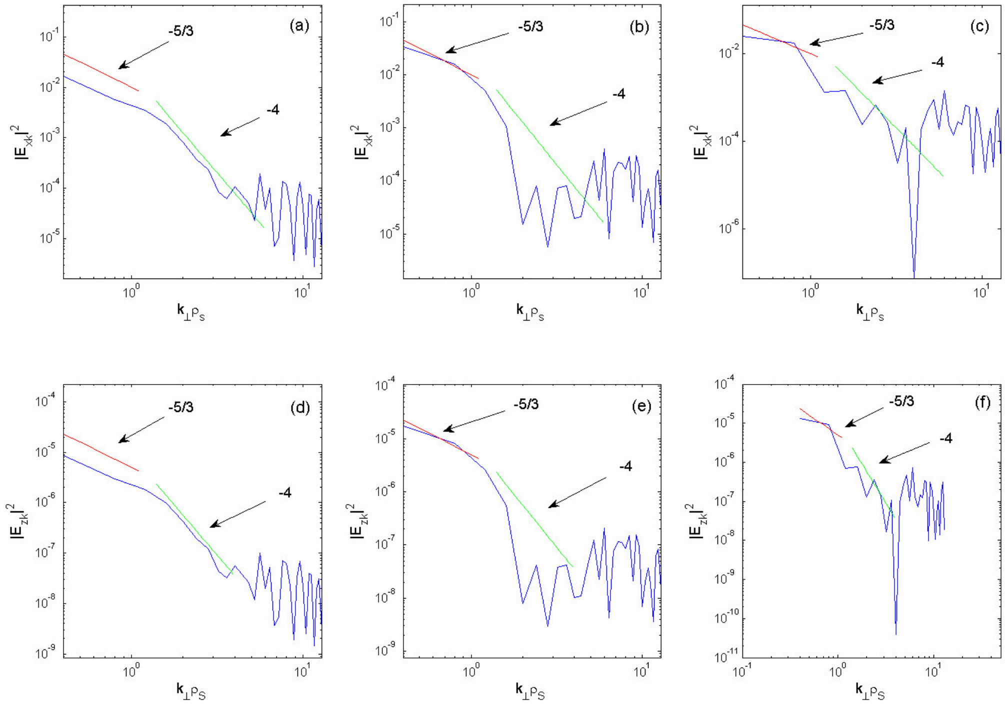

Fig. 9 Spectra of electric field fluctuations for IC-1 in $k_\perp$ space: perpendicular electric field (*upper panels*) and parallel electric field (*lower panels*) at $t = 2, 3$ and 4.

tion (instead of cosine perturbation in IC-1) on a uniform plane wave. Almost the same pattern of filament formation is seen but at different times, locations and intensities. At times $t = 3, 4$ and 6, the filaments with highest intensities are around 30, 23 and 13 respectively. The contour plots connecting the same magnetic field energies in the (k_x, k_z) plane are depicted in Figure 2(d)–2(f). In Figure 3(a)–3(c), the snapshots of magnetic field intensity profiles for IC-3, a cosine perturbation to a Gaussian wavefront, are displayed. At $t = 6.5, 8$ and 9.5, the highest intensity magnetic filaments are around $1.30, 0.40$ and 1.36, respectively. From this we can conclude that although low intensity filaments can be formed, higher intensity filaments cannot be formed in case of IC-3. From Figure 3(d)–3(f), it is evident that the energy cannot be distributed much to other higher wavenumbers. Therefore, this kind of nonuniformity (IC-3) in magnetic field may not be appropriate to sufficiently heat the solar corona. The simulation results for IC-4, a random perturbation to a Gaussian wavefront, manifest almost similar results with those of IC-3, as displayed in Figure 4. From these results we can conclude that the magnetic intensity profile is mainly dependent on the nature of the pump KAW. For the same pump KAW wavefront with different perturbing waveforms, there is little variation in the intensity profile in terms of magnetic intensity and its locations and the evolution time of filament formation. If we compare the evolution times when the proper filaments start forming, they start at earlier times for IC-1 (i.e. $t = 2$) and IC-2 ($t = 3$), but at later times for IC-3 ($t = 6.5$) and IC-4 ($t = 5$). Since for all initial conditions, the intensities of filaments are different, we expect non-similarities in the distribution of energies in different wavenumbers, which are exemplified in the depictions appearing on the lower panels of Figure 1–4. This will be more reflected in the spectral scaling of the wavenumber spectra that we are going to discuss below.

From the simulation results of localization, it has been found that the transverse scale size of the localized structures or filaments of KAWs are localized in space covering all scales from the energy injection scale (when the size of a filament is comparable to ion gyroradius/ion inertial length) to dissipation scale (when the size of a filament is comparable to electron gyroradius/electron inertial length). Let us make an analogy between the the generation of magnetic coherent structures and the phenomenon of laser focusing (Kruer 2013). If there are variations in the density of a medium, the dielectric constant of the medium will also be varied. It will produce changes in the refractive index. When a laser beam propagates through a medium of varying refractive index, the medium will behave like a focusing lens. Therefore a focused laser beam will be produced. In a similar way, the parallel ponderomotive force in the solar plasma will generate perturbations in the density. When the KAWs propagate through the plasma, their phase velocity will change and it will lead to the localization of KAWs.

When the nonlinearities arising from inhomogeneities in the field and density are combined with the imbalance in the number of particles moving faster than the wave, plasma heating occurs (Gershman et al. 2017). If the parallel fluctuations in fields and current density are large enough, the charged particles (electrons) can be trapped in between the wave packets. As the wave propagates, the wave's kinetic energy is transferred to particle energy leading to the magnetic analog of Landau damping. The ion motions decouple from the electron motions when the wave packet (filament) sizes are smaller than that of ion acoustic gyroradius ρ_s. From the snapshots of magnetic field profile, at the early evolution times the transverse filament sizes are of the order of ion gyroradius $\approx 6\rho_s = 188.50\,$km at half of the peak intensity. At later evolution times, when the transverse collapse happens, this filamentary size becomes much smaller, leading to kinetic scales of KAWs, thereby heating the plasma particles. Many authors (Lion et al. 2016; Chmyrev et al. 1988) found the KAW filamentary size of the order of ρ_s. In our present dynamical equation, if we increase the pump wave amplitude by increasing the parameter g as carried out by Sharma et al. (2006) in the steady state model, the filamentary size becomes less than ρ_s. When the microscale kinetic scales of the particles such as ρ_s are comparable to the short perpendicular wavelength of the KAWs, wave-particle energy exchange happens to effectively heat the plasma.

Further along with the localization of KAWs, we have studied the transfer of energy in wavenumber spectra by plotting $|B_{yk}|^2$ against $k_x(k_\perp)$ and $k_z(k_\parallel)$. The saturated power spectra of KAWs at different times were plotted by averaging over all parallel wavenumbers when the system reaches quasi-steady state. It is clearly shown from Figures 5–8 that for all the initial conditions up to $k_\perp\rho_s < 1$ and $k_\parallel\rho_s < 1$ (inertial range), the energy cascade follows the Kolmogorov scaling with spectral index $-5/3$ as observed by many authors (Champeaux et al. 1998; Laveder et al. 2001; Sulem & Sulem 1999). There are observations from solar flares (Dennis 1985; Hudson 1991) which manifest power law spectral index of -1.6. Hollweg (1984) suggested that the dissipation of AWs via a turbulent energy cascade to high wavenumbers with Kolmogorov scaling may be responsible for heating of the coronal loops. The energy flux density in the coronal loops was calculated using the Kolmogorov scale of turbulence and it was found to be consistent with observations. Although this energy flux was sufficient to heat the coronal loops, the physical processes responsible for turbulence are not as yet fully understood. The transverse collapse of the magnetic filaments of KAWs has been proposed here as one of the candidates to explain the Kolmogorov turbulence as well as the dissipation of coronal loop energy via high wavenumbers that can heat the corona.

From the power spectra, the first spectral break was found at $k_\perp\rho_s \approx 1$ and $k_\parallel\rho_s \approx 1$ showing no fixed spectral slopes for the initial conditions of magnetic field inhomogeneity. This break is the transition region from inertial range (ion scale) to kinetic range (electron scale). In our case, we found the spectral indices in $k_\perp$ to be -3.2 and -4 for IC-1, -4 for IC-2, -10 for IC-3 and -2.7 for IC-4. The spectral indices in $k_\parallel$ are -6 and -8 for IC-1, -8 for IC-2, -12 for IC-3 and -9 for IC-4. For sufficient heating of the solar corona by small scale bursts such as solar flares, Hudson (1991) pointed out the spectral slope needs to be more negative than -2. By analyzing the data from many spacecrafts such as *Yohkoh* with SXT, *SOHO* and *TRACE*, the spectral power index of small-scale brightenings in the quiet-Sun and active regions was steeper than -2 (e.g. Aschwanden & Parnell 2002). In our case, it is evident from Figures 5–8 that the spectral slope is deeper in $k_\parallel$ in comparison to the slope in $k_\perp$. This means less energy is cascading in parallel wavenumber space. Such kind of fluctuations in the power spectra play a very important role in transferring energy and heating the solar corona, indicating the distribution of energy among intermediate and high wavenumbers. Early studies of weak MHD turbulence predicted the non-cascade of energy in parallel wavenumber space (Kraichnan 1965; Shebalin et al. 1983). Later, cascade of energy in the parallel wavenumber space was evident from many studies in the strong MHD turbulence regime (Goldreich & Sridhar 1995). So, the magnetic field direction can induce anisotropy in the solar plasma turbulence. By utilizing numerical simulations in 2D and 3D, many authors (Shebalin et al. 1983; Oughton et al. 1994; Milano et al. 2001) have demonstrated the wavevector anisotropy in plasma turbulence resulting in $k_\perp >> k_\parallel$. As is also evident from our Figures 5–8 by comparing the upper and lower panels, the spectral anisotropy is present for the parameters applied in the simulation for coronal loops. The anisotropic magnetic fluctuations with respect to the mean magnetic field in the kinetic small scale regime were reported by many authors (Chen et al. 2010; Sahraoui et al. 2010; Narita et al. 2011). The anisotropic turbulence is more significant at large wavenumbers. The energy is cascaded more in the transverse wavenumber, i.e. when $k_\perp > k_\parallel$. In our results, by examining Figures 5–8, it was found that the magnetic spectral slope in the kinetic small scale is deeper along $k_\parallel$ in comparison to that along $k_\perp$. This indicates that more intensity of energy is cascaded along the perpendicular wavenumber space in comparison to the energy cascaded along the parallel wavenumber space. Out of the four initial conditions, IC-3 results in the least cascade of energy to higher wavenumbers. Therefore, the shape of the power spectra in perpendicular and parallel wavenumber space will not be same. Various numerical studies (Maron & Goldreich 2001; Cho et al. 2002) and spacecraft data (Leamon et al. 1998; Luo & Wu 2010; Luo et al. 2011) confirmed the anisotropically cascading model of KAW turbulence. Many authors have found the anisotropic scaling of KAWs as $k_\parallel \propto k_\perp^{1/3} (= k_\perp^{0.33})$ (Schekochihin et al. 2009; Cho & Lazarian 2004; Cho & Lazarian 2009). Our wavenumber spectra also show the anisotropic scaling as nearly as $k_\parallel \propto k_\perp^{0.53}$ and $k_\parallel \propto k_\perp^{0.50}$ for IC-1 and IC-2; $k_\parallel \propto k_\perp^{0.83}$ for IC-3 and $k_\parallel \propto k_\perp^{0.30}$ for IC-4. Considering the effects of anisotropic dispersion and turbulence, the KAW turbulence cascades in parallel and perpendicular wavenumber space need to be investigated properly to understand the coronal heating problem.

Because of the transverse collapse of magnetic coherent structures, the nonlinear energy transfer is maximized for the transverse directions, thereby characterizing the extension or elongation of the energy spectrum preferentially across the ambient magnetic field. The energy is preferentially cascading towards smaller scales across the mean field direction rather than in the parallel direction. So, the perpendicular wavevector component of the fluctuations increases, resulting in wavevector anisotropy. Here we have taken the initial conditions of the simulations as a perturbation superimposed on a main KAW. The perturbation associated with the pump wave takes the energy away from the main KAW and after having sufficient energy, the coherent magnetic structures collapse with the evolution of time. From the numerical simulations we see that the localized structures are strongly dependent on the form of the main KAW. In case of IC-1 and IC-2, the main KAW is a uniform plane wavefront with a fixed initial amplitude. This plane wavefront superimposed with periodic/Gaussian waveforms may be able to give intense filaments to heat the plasma more in the transverse direction. On the other hand, for IC-3 and IC-4, the main KAW is a Gaussian wavefront whereas it may not be able to give intense filaments in comparison to IC-1 and IC-2, so the heating across the magnetic field is relatively low. One can also consider the semi-analytical solutions with pre-assumed trial inhomogenous fields in the form of four initial conditions studied here and calculate the growth rate of KAW instability and its dependence on wavevectors. Such analysis will shed light on the role of different initial conditions in the wavevector anisotropy. In addition, the filamentation process can create conditions favorable for other instabilities. Since it has the lowest instability thresholds, it can increase the growth rate of other instabilities which may be responsible for transfer of energies. However, we do not observe a single unique spectral slope for different initial conditions. This suggests that the evolution of the turbulent fluctuations presented here does not represent a state of fully developed turbulence. Moreover, the exact nature of spectral slopes, the generation of anisotropic turbulence with different fluctuation power in parallel and perpendicular wavenumber spaces, is a tedious problem which requires more studies for better understanding.

Finally, we study the spectral structures of perpendicular and parallel electric field fluctuations resulting from KAW turbulence cascading in the perpendicular wavenumber space. From Equations (13) and (14), the normalized E_x and E_z are $E_x = (2 - e^{|B_y|^2})B_y$ and $E_z = B_y/Q$, respectively, where $Q = v_A^2/(v_{te}^2 \lambda_e^2 k_{0x} k_{0z})$ is a dimensionless constant and the electric field is normalized by $E_N = B_N k_{0z} v_A^2/(\omega c)$. In Figure 9, we can see that both the spectra have spectral indices of $k^{-5/3}$ for inertial range and k^{-4} for dissipation range. The spectral indices for the electric field are quite similar to those of magnetic spectral indices except that the spectral intensity for the parallel electric field is smaller than that of the perpendicular electric field, so we are showing it only for IC-1. Zhao et al. (2016) have developed a semi-phenomenological model of Alfvénic turbulence and found the turbulent scaling of $k_\perp^{-5/3}$ and $k_\perp^{-1/3}$ for perpendicular electric spectra in the intermediate (kinetic) beta regime, while they found $k_\perp^{4/3}$ and $k_\perp^{-1/3}$ for parallel electric spectra. For scales smaller than the ion kinetic scales $k\rho_i > 1$, many authors (Schekochihin et al. 2009; Zhao et al. 2013; Bian & Kontar 2010) have also predicted a scaling of $k_\perp^{-1/3}$ and by considering the strong intermittency, Boldyrev & Perez (2012) predicted the scaling of $-2/3$. For a parallel electric spectrum, Zhao et al. (2016) identified the spectral indices of $k_\perp^{4/3}$ and $k_\perp^{-1/3}$ in the inertial and kinetic scales respectively. The parallel electric energy increases with the perpendicular wavenumber in the inertial range (Zhao et al. 2013; Bian & Kontar 2011) as the turbulence cascades to smaller scales. However, they did not find a proper definite spectral shape for kinetic scales. Mozer & Chen (2013) showed from the *THEMIS* and *Cluster* data that the perpendicular and parallel electric spectra have similar shapes and amplitudes with power laws with exponents near $-5/3$ below the ion scales and flat spectra at the vicinity of this scale. At small scales, the spectra manifested steep spectral indices ranging from -2.1 to -2.8. However, many other authors (Zhao et al. 2013; Bian & Kontar 2010; Bian & Kontar 2011; Mozer & Chen 2013) have shown that the spectral amplitudes of the parallel electric field are much lower than those of perpendicular electric field spectral energy. Therefore, the main contribution to the total electric field spectrum is due to the perpendicular electric field.

From Figure 9, we see that the parallel electric field energy is smaller by an order of 3 than the perpendicular electric field energy. However, it should be noted that the parallel electric field is the actual force which mediates the wave-particle interaction and can play an important role in electron energization (Wu & Fang 1999; Fletcher & Hudson 2008; McClements & Fletcher 2009) via Landau resonance. It happens when the electric thermal speeds are comparable to the wave phase velocity $v_{ph} = \omega/k_{\|}$ and hence increasing the process of turbulence cascading to smaller scales. This resonant acceleration process is a diffusion in velocity space and can be treated under stochastic resonant heating with quasilinear theory. The parallel electric field spectrum we generate can be effectively used to model the stochastic resonant acceleration with quasilinear theory.

In our case, the parallel and perpendicular electric field spectra at dissipative range are steeper than some predictions (Bian & Kontar 2010; Bian et al. 2010; Mozer & Chen 2013) but agree qualitatively with results from hybrid Vlasov-Maxwell simulations (Valentini et al. 2017) by imposing Alfvénic perturbations on an initial pressure-balanced magnetic shear equilibrium and gyrokinetic continuum simulations (Howes et al. 2008; Howes et al. 2011).

From the magnetic spectra, we see that at the scale length of electron inertial length, i.e. $k_{\perp}\rho_s \approx 5$, and $k_{\|}\rho_s \approx 5$, there is a second break point in the spectral index. It should be mentioned here that the present study is not valid in this region because our KAW dynamics were developed for $\omega < \omega_{ci}$. On the other hand, at scales close to ρ_s/ρ_e, wave particle interactions lead to Landau damping (Gary & Nishimura 2004; Sahraoui et al. 2009). In the electron scale region, whistler mode $\omega > \omega_{ci}$ is more relevant. From the cluster spacecraft data of solar wind, Sahraoui et al. (2009) demonstrated that the cascade of energy is carried by KAWs with $\omega < \omega_{ci}$ down to $k_{\perp}\rho_i \approx 10$, corresponding to a frequency of around 5 Hz. The region beyond this was limited by the noise level of the instrument. Dwivedi & Sharma (2013) studied the anisotropic scaling in wavenumber power spectra by considering the presence of both KAW mode and whistler mode. However, the origin of small scale fluctuations is not understood well, which may be due to whistler waves or KAWs, or the interactions between them (Gary & Smith 2009; Salem et al. 2012; Boldyrev et al. 2013; Chen et al. 2013a,b) or interactions of KAWs with ion acoustic and magnetosonic waves. Sharma et al. (2017) also studied coronal heating by considering the localization of slow magnetosonic waves due to the background density perturbation. In spite of all these mechanisms, there is still no consensus theory to explain the coronal heating by turbulence. Therefore, our transient KAW dynamics with modified background density due to ponderomotive force and Joule heating, leading to the transverse collapse of magnetic coherent structures may be one of the possible physical process to explain the heating in coronal loops.

4 CONCLUSIONS

In summary, we have presented the numerical simulation results of modified NLSE satisfying the transient KAWs propagating in an inhomogenous coronal loop plasma. The dynamical field equation couples with the field aligned density perturbations arising because of ponderomotive force and Joule heating. The nonlinearity in the field equation leads to the localization of KAW wave packet as envelope solitons. As the wave propagates, the transverse collapse of the coherent structures happens, giving rise to turbulence. The spectral power indices are deeper in $k_{\|}$ in comparison to the indices in $k_{\perp}$. This means less energy is cascading in parallel wavenumber space. Such kind of fluctuations in the power spectra plays a very important role in transferring the energy and heating the solar corona, indicating the distribution of energy among intermediate and high wavenumbers. The saturated magnetic power spectra follow Kolmogorov scaling of $k^{-5/3}$ in the inertial range, then followed by steep anisotropic scaling in the dissipation range. The KAW has anisotropy of $k_{\|} \propto k_{\perp}^{0.53}$, $k_{\|} \propto k_{\perp}^{0.50}$, $k_{\|} \propto k_{\perp}^{0.83}$ and $k_{\|} \propto k_{\perp}^{0.30}$ depending on the kind of initial conditions of inhomogeneity. The power spectra of magnetic field fluctuations showing the spectral anisotropy in wavenumber space indicate that the nonlinear interactions may be redistributing the energy anisotropically among higher modes of the wavenumber. Therefore, anisotropic turbulence can be considered as one of the candidates responsible for the particle energization and heating of the solar plasmas.

Acknowledgements Bheem Singh Jatav is grateful to UGC for providing RGNF for doing research work.

References

Alfvén, H. 1942, Nature, 150, 405
Aschwanden, M. J., & Parnell, C. E. 2002, ApJ, 572, 1048
Asgari-Targhi, M., & van Ballegooijen, A. A. 2012, ApJ, 746, 81
Bellan, P. M., & Stasiewicz, K. 1998, Physical Review Letters, 80, 3523
Bian, N. H., & Kontar, E. P. 2010, Physics of Plasmas, 17, 062308
Bian, N. H., Kontar, E. P., & Brown, J. C. 2010, A&A, 519, A114
Bian, N. H., & Kontar, E. P. 2011, A&A, 527, A130
Boldyrev, S., Horaites, K., Xia, Q., & Perez, J. C. 2013, ApJ, 777, 41
Boldyrev, S., & Perez, J. C. 2012, ApJ, 758, L44

Cassak, P. A., & Shay, M. A. 2012, Space Sci. Rev., 172, 283
Champeaux, S., Gazol, A., Passot, T., et al. 1997, ApJ, 486, 477
Champeaux, S., Passot, T., & Sulem, P. L. 1998, Physics of Plasmas, 5, 100
Chen, Y., Li, Z.-y., Liu, W., & Shi, Z.-D. 2000, Physics of Plasmas, 7, 371
Chen, C. H. K., Horbury, T. S., Schekochihin, A. A., et al. 2010, Physical Review Letters, 104, 255002
Chen, C. H. K., Boldyrev, S., Xia, Q., & Perez, J. C. 2013a, Physical Review Letters, 110, 225002
Chen, L., Wu, D. J., & Huang, J. 2013b, Journal of Geophysical Research (Space Physics), 118, 2951
Chmyrev, V. M., Bilichenko, S. V., Pokhotelov, O. A., et al. 1988, Phys. Scr, 38, 841
Cho, J., Lazarian, A., & Vishniac, E. T. 2002, ApJ, 564, 291
Cho, J., & Lazarian, A. 2004, ApJ, 615, L41
Cho, J., & Lazarian, A. 2009, ApJ, 701, 236
Cirtain, J. W., Golub, L., Lundquist, L., et al. 2007, Science, 318, 1580
Cranmer, S. R., van Ballegooijen, A. A., & Edgar, R. J. 2007, ApJS, 171, 520
Cranmer, S. R. 2009, Living Reviews in Solar Physics, 6, 3
Cravens, T. E. 2004, Physics of Solar System Plasmas, (2nd ed., New York: Cambridge Univ. Press)
de Azevedo, C. A., Elfimov, A. G., & de Assis, A. S. 1994, Sol. Phys., 153, 205
De Pontieu, B., McIntosh, S. W., Carlsson, M., et al. 2007, Science, 318, 1574
Dennis, B. R. 1985, Sol. Phys., 100, 465
Dwivedi, N. K., & Sharma, R. P. 2013, Physics of Plasmas, 20, 042308
Elfimov, A. G., de Azevedo, C. A., & de Assis, A. S. 1996, Physica Scripta Volume T, 63, 251
Fletcher, L., & Hudson, H. S. 2008, ApJ, 675, 1645
Gary, S. P., & Nishimura, K. 2004, Journal of Geophysical Research (Space Physics), 109, A02109
Gary, S. P., & Smith, C. W. 2009, Journal of Geophysical Research (Space Physics), 114, A12105
Gekelman, W., Pribyl, P., Palmer, N., et al. 1999, in APS Division of Plasma Physics Meeting Abstracts, 41, CP1.53
Génot, V., Louarn, P., & Le Quéau, D. 1999, J. Geophys. Res., 104, 22649
Génot, V., Louarn, P., & Mottez, F. 2004, Annales Geophysicae, 22, 2081
Gershman, D. J., F-Viñas, A., Dorelli, J. C., et al. 2017, Nature Communications, 8, 14719
Goldreich, P., & Sridhar, S. 1995, ApJ, 438, 763
Goldreich, P., & Sridhar, S. 1997, ApJ, 485, 680
Goossens, M. 1994, Space Sci. Rev., 68, 51
Hasegawa, A., & Chen, L. 1975, Physical Review Letters, 35, 370
Hollweg, J. V. 1984, ApJ, 277, 392
Hood, A. W., Browning, P. K., & van der Linden, R. A. M. 2009, A&A, 506, 913
Hood, A. W., Ireland, J., & Priest, E. R. 1997, A&A, 318, 957
Howes, G. G., Cowley, S. C., Dorland, W., et al. 2006, ApJ, 651, 590
Howes, G. G., Dorland, W., Cowley, S. C., et al. 2008, Physical Review Letters, 100, 065004
Howes, G. G., Tenbarge, J. M., Dorland, W., et al. 2011, Physical Review Letters, 107, 035004
Hudson, H. S. 1991, Sol. Phys., 133, 357
Jain, R., Browning, P., & Kusano, K. 2005, Physics of Plasmas, 12, 012904
Kraichnan, R. H. 1965, Physics of Fluids, 8, 1385
Kruer, William, L. 2013, Physics of Laser Plasma Interactions (Westview Press)
Laveder, D., Passot, T., & Sulem, P. L. 2001, Physica D Nonlinear Phenomena, 152, 694
Leamon, R. J., Smith, C. W., Ness, N. F., et al. 1998, J. Geophys. Res., 103, 4775
Lion, S., Alexandrova, O., & Zaslavsky, A. 2016, ApJ, 824, 47
Luo, Q. Y., & Wu, D. J. 2010, ApJ, 714, L138
Luo, Q. Y., Wu, D. J., & Yang, L. 2011, ApJ, 733, L22
Maron, J., & Goldreich, P. 2001, ApJ, 554, 1175
Marsch, E. 2006, Living Reviews in Solar Physics, 3, 1
McClements, K. G., & Fletcher, L. 2009, ApJ, 693, 1494
Milano, L. J., Matthaeus, W. H., Dmitruk, P., et al. 2001, Physics of Plasmas, 8, 2673
Morton, R. J., Tomczyk, S., & Pinto, R. 2015, Nature Communications, 6, 7813
Mottez, F., Génot, V., & Louarn, P. 2006, A&A, 449, 449
Mottez, F., & Génot, V. 2011, Journal of Geophysical Research (Space Physics), 116, A00K15
Mozer, F. S., & Chen, C. H. K. 2013, ApJ, 768, L10
Narain, U., & Ulmschneider, P. 1996, Space Sci. Rev., 75, 453
Narita, Y., Gary, S. P., Saito, S., et al. 2011, Geophys. Res. Lett., 38, L05101
Okamoto, T. J., Tsuneta, S., Berger, T. E., et al. 2007, Science, 318, 1577
Oughton, S., Priest, E. R., & Matthaeus, W. H. 1994, Journal of Fluid Mechanics, 280, 95
Parker, E. N. 1979, Cosmical Magnetic Fields: Their Origin and Their Activity (Oxford: Clarendon)
Poedts, S., Goossens, M., & Kerner, W. 1989, Sol. Phys., 123, 83
Priest, E. R., Foley, C. R., Heyvaerts, J., et al. 2000, ApJ, 539, 1002
Ruderman, M. S. 1999, ApJ, 521, 851
Sahraoui, F., Goldstein, M. L., Robert, P., & Khotyaintsev, Y. V. 2009, Physical Review Letters, 102, 231102
Sahraoui, F., Goldstein, M. L., Belmont, G., Canu, P., & Rezeau, L. 2010, Physical Review Letters, 105, 131101
Salem, C. S., Howes, G. G., Sundkvist, D., et al. 2012, ApJ, 745, L9
Schekochihin, A. A., Cowley, S. C., Dorland, W., et al. 2009, ApJS, 182, 310

Sharma, R. P., Singh, H. D., & Malik, M. 2006, Journal of Geophysical Research (Space Physics), 111, A12108

Sharma, R. P., & Kumar, S. 2011, Journal of Geophysical Research (Space Physics), 116, A03103

Sharma, R. P., Yadav, N., & Pathak, N. 2014, Ap&SS, 351, 75

Sharma, P., Yadav, N., & Sharma, R. P. 2016, Physics of Plasmas, 23, 052304

Sharma, R. P., Sharma, P., & Yadav, N. 2017, Physics of Plasmas, 24, 012905

Shebalin, J. V., Matthaeus, W. H., & Montgomery, D. 1983, Journal of Plasma Physics, 29, 525

Shukla, P. K., Bingham, R., McKenzie, J. F., & Axford, W. I. 1999a, Sol. Phys., 186, 61

Shukla, P. K., Stenflo, L., & Bingham, R. 1999b, Physics of Plasmas, 6, 1677

Shukla, P. K., & Stenflo, L. 1999, Physics of Plasmas, 6, 4120

Shukla, P. K., & Stenflo, L. 2000a, Physics of Plasmas, 7, 2747

Shukla, P. K., & Stenflo, L. 2000b, Physics of Plasmas, 7, 2738

Shukla, P. K., & Stenflo, L. 2005, Physics of Plasmas, 12, 084502

Singh, H. D., & Jatav, B. S. 2019, RAA (Research in Astronomy and Astrophysics), 19, 093

Singh, H. D., & Sharma, R. P. 2007, Physics of Plasmas, 14, 102304

Sirenko, O., Voitenko, Y., & Goossens, M. 2002, A&A, 390, 725

Stéfant, R. J. 1970, Physics of Fluids, 13, 440

Sturrock, P. A., Roald, C. B., & Wolfson, R. 1999, ApJ, 524, L75

Sulem, C., & Sulem, P. L. 1999, Applied Mathematical Sciences, 139 (New York: Springer)

Testa, P., De Pontieu, B., Allred, J., et al. 2014, Science, 346, 1255724

Tsiklauri, D., Sakai, J.-I., & Saito, S. 2005, A&A, 435, 1105

Tsiklauri, D., & Haruki, T. 2008, Physics of Plasmas, 15, 112902

Tsiklauri, D. 2011, Physics of Plasmas, 18, 092903

Tsiklauri, D. 2012, Physics of Plasmas, 19, 082903

Valentini, F., Vásconez, C. L., Pezzi, O., et al. 2017, A&A, 599, A8

Voitenko, Y., & Goossens, M. 2004, ApJ, 605, L149

Voitenko, Y. M. 1995, Sol. Phys., 161, 197

Voitenko, Y. M. 1996, Sol. Phys., 168, 219

Voitenko, Y. M. 1998, Sol. Phys., 182, 411

Wang, X.-Y., Wang, X.-Y., Liu, Z.-X., & Li, Z.-Y. 1998, Physics of Plasmas, 5, 4395

Wu, D. J., & Fang, C. 2003, ApJ, 596, 656

Wu, D. J., & Fang, C. 2007, ApJ, 659, L181

Wu, D. J., Wang, D. Y., & Huang, G. L. 1997, Physics of Plasmas, 4, 611

Wu, D. J., & Fang, C. 1999, ApJ, 511, 958

Wu, D. J., & Yang, L. 2006, A&A, 452, L7

Wu, D. J., & Yang, L. 2007, ApJ, 659, 1693

Wu, D. J., & Chen, L. 2013, ApJ, 771, 3

Zhao, J. S., Voitenko, Y. M., Wu, D. J., & Yu, M. Y. 2016, Journal of Geophysical Research (Space Physics), 121, 5

Zhao, J. S., Wu, D. J., & Lu, J. Y. 2013, ApJ, 767, 109

Zhou, C., & He, X. T. 1994, Phys. Rev. E, 49, 4417

Zhou, C., He, X. T., & Chen, S. 1992, Phys. Rev. A, 46, 2277